POWDER CHARACTERISTICS BLENDING AND MICROSTRUCTURAL ANALYSIS OF A HOT-PACK ROLLED VACUUM ARC-MELTED γ-TIAL-BASED SHEET

J. J. M. Ellard[1,2], M. N. Mathabathe[2*], C. W. Siyasiya[1] & A. S. Bolokang[2,3]

ARTICLE INFO

Article details
Presented at the 23rd Annual International Conference of the Rapid Product Development Association of South Africa (RAPDASA) Institute for Industrial Engineering, held from 9 to 11 November 2022 in Somerset West, South Africa

Available online 11 Nov 2022

Contact details
* Corresponding author
nmathabathe@csir.co.za

Author affiliations
1 Department of Material Science and Metallurgical Engineering, University of Pretoria, Pretoria, South Africa

2 Manufacturing Cluster, Advance Materials Engineering, Council of Scientific Industrial Research, South Africa

3 Department of Physics, University of the Western Cape, Bellville, South Africa

ORCID® identifiers
J. J. M. Ellard
0000-0001-7025-4792

M. N. Marhabarthe
0000-0001-7058-5647

C. W. Siyasiya
0000-0002-1426-3149

A. S. Bolokang
0000-0003-1879-0445

DOI
http://dx.doi.org//10.7166/33-3-2809

ABSTRACT

In the quest for cost-effective fabrication processes capable of producing sound γ-TiAl products, the microstructure and mechanical properties of a modified second-generation hot-rolled γ-TiAl-based alloy with nominal composition Ti-48Al-2Nb-0.7Cr-0.3Si were investigated in this work. The alloy was fabricated using a processing route that involved uniaxial cold-pressing of powders and vacuum arc re-melting. Prior to the cold pressing, the elemental powder characteristics, such as particle sizes and morphologies, were blended to minimise porosity in the compact that might be inherited by the final ingot. A hot-pack rolling process was carried out directly from the melted button-ingot using a conventional two-high rolling mill to produce a 4 mm-thick sheet. The relative density results of both as-compacted and as-melted alloy parts showed a significant reduction of porosity in the alloy. In addition, both the optical and the scanning electron microscopy micrographs of the rolled sheet revealed a typical 'duplex' microstructure with a mean grain size of about 9 μm. Moreover, the results from a room-temperature indentation plastometry test of the hot-rolled sheet indicated good mechanical properties with recorded yield strength of about 600 MPa, an ultimate tensile strength of about 850 MPa, and a true plastic strain of about 3%.

OPSOMMING

In 'n soektog na koste-effektiewe vervaardigingsprosesse wat in staat is om goeie γ-TiAl-produkte te produseer, is die mikrostruktuur en meganiese eienskappe van 'n gemodifiseerde tweedegenerasie warmgewalste γ-TiAl-gebaseerde legering met nominale samestelling Ti-48Al-2Nb-0.7Cr-0.3Si ondersoek. Die legering is vervaardig deur gebruik te maak van 'n verwerkingsroete wat eenassige koue pers van poeiers en vakuumbooghersmelting behels. Voor die koue pers is die elementêre poeierkenmerke, soos deeltjiegroottes en morfologieë, vermeng om porositeit in die kompak te minimaliseer wat deur die finale steen geërf kan word. 'n Warmpak-walsproses is direk vanaf die gesmelte knoppiesblok uitgevoer met behulp van 'n konvensionele twee-hoë walswerk om 'n 4 mm-dik plaat te vervaardig. Die relatiewe digtheidsresultate van beide as-saamgepakte en as-gesmelte legeringsdele het 'n beduidende vermindering van porositeit in die legering getoon. Daarbenewens het beide die optiese en die skandeer-elektronmikroskopie mikrograwe van die gerolde vel 'n tipiese "dupleks" mikrostruktuur met 'n gemiddelde korrelgrootte van ongeveer 9 μm geopenbaar. Boonop het die resultate van 'n kamertemperatuur inkepingsplastometrietoets van die warmgewalste plaat goeie meganiese eienskappe met aangetekende vloeisterkte van ongeveer 600 MPa, 'n uiteindelike treksterkte van ongeveer 850 MPa en 'n ware plastiese vervorming van ongeveer 3% aangedui.

1. INTRODUCTION

Interesting properties qualify γ-TiAl-based alloys as the potential materials to replace heavy materials in the aerospace and automobile industries [1]. However, the materials inherently lack low-temperature ductility and have low values of toughness. Owing to their brittle nature, care must be taken to ensure that their processing routes avoid any form of defects such as porosity, inclusions, cracks, and segregation that could induce premature rupture of the components. This, therefore, makes it almost impractical to produce sound products cost-effectively that are made of γ-TiAl-based alloys using conventional processing methods – viz., investment casting and ingot metallurgy [2], [3].

To address these challenges related to the processing of these alloys, other fabrication processes that are capable of producing acceptable products at a lower fabrication cost must be explored to promote the use of γ-TiAl-based alloys as economically feasible structural materials. To this end, Mathabathe et al. [4] successfully fabricated alloys with nominal composition Ti-48Al, Ti-48Al-2Nb and Ti-48Al-2N-0.7Cr, using a fabrication route that incorporated powder metallurgy to produce green compacts at room temperature and using an ingot metallurgy technique known as vacuum arc re-melting (VAR) to melt the green compacts into ingots. Nevertheless, as emphasised by the researchers, 100% densification of the as-melted alloys could not be achieved owing to the presence of shrinkage cavities in the resulting ingots [4]. Therefore, the ingot quality needed to be improved to minimise the presence of the cavities and so improve the mechanical properties.

Still, the improvement of ingot quality alone is not enough to bestow the desirable mechanical properties on these inherently brittle materials. Therefore, methods that can refine the microstructure and impart optimised properties to the final product must be considered. Of all the existing methods of microstructural refinement, hot-working is regarded as the most attractive and efficient way of getting product forms – viz., pancakes, extrusions, and sheets – that possess balanced mechanical properties [5].

With regard to the production of γ-TiAl-based sheets, processing approaches involving powder and ingot metallurgy have been developed and applied to alloy systems [6], [7]. However, for the powder metallurgy (P/M) route, hot isostatic pressing of the powder is the key to achieving full densification. Furthermore, given the tendency of the inert argon gas to be entrapped in powder particles, the fabricated sheet material normally contains thermally induced porosity [6]. Concerning the ingot metallurgy (I/M) route for manufacturing γ-TiAl-based sheets, Shen et al. [5] stated that, unless the cast ingot undergoes a series of thermo-mechanical processes prior to further processing, it could contain an unacceptable level of porosity. These intermediate thermo-mechanical processes lead to complex processes that require special equipment as far as the fabrication of γ-TiAl-based sheets is concerned, thus rendering the entire production process less cost-effective for most of the applications.

Therefore, the current study aimed to investigate the microstructure and mechanical properties of a γ-TiAl-based sheet that was fabricated using the processing route that involved uniaxial cold-pressing of the powders, followed by vacuum arc re-melting, then direct hot pack rolling [5] of the resulting ingot. It was interesting to note that the powder pressing was carried out at room temperature instead of using hot isostatic pressing (HIPing), and the hot-rolling was conducted directly on the as-cast ingot using a conventional two-high mill without performing any intermediate thermo-mechanical processes. Powder characteristics such as particle morphologies and sizes were blended prior to uniaxial cold-pressing to promote mechanical interlocking of the particles, and to ensure that the gaps between particles were reduced.

2. EXPERIMENTAL WORK

2.1. Materials preparation

A γ-TiAl-based alloy of a nominal composition Ti-48Al-2Nb-0.7Cr-0.3Si (at. %) was studied in this work. The elemental powders with the average particle sizes and shapes shown in Table 1, with a total quantity of 70 g, were blended and mixed in a tubular mixer for 30 minutes to promote even chemical distribution. Subsequently, the powder charge was compressed uniaxially at room temperature with an applied pressure of 380 MPa [4] on an Enerpac hydraulic press to produce a cylindrical green compact of 53 mm diameter with 11.5 mm length. The compact was then melted under a vacuum of 1×10^{-5} Torr in

an electric arc melting furnace to produce a button-ingot of dimensions 38 × 38 × 13 mm^3. The same fabrication process was reported in [8].

2.2. Hot pack-rolling

The button-ingot was encapsulated in a stainless steel case directly after arc-melting to prevent it from cracking as a result of the large temperature gradient between the ingot and the mill rolls. To avoid bonding the ingot and the case during the rolling process, the ingot-case interface was filled with zirconia powder. The case was sealed by tungsten inert gas (TIG) welding. Finally, the assembly was heated within the safe deformation region for the alloy at 1280 °C [9] for one hour, and then rolled on a two-high mill with rolls of 300 mm diameter at a speed of 2 mm s^{-1} with a thickness reduction of about 25% per pass to reduce the thickness to 4 mm, followed by air cooling. After each pass, the specimen was reheated to 1280 °C and held at this temperature for 20 minutes. After rolling, a specimen was cut from the rolled sheet and heat-treated at 1250 °C for one hour, and then furnace-cooled. The schematic representation of the rolling process is shown in Figure 1.

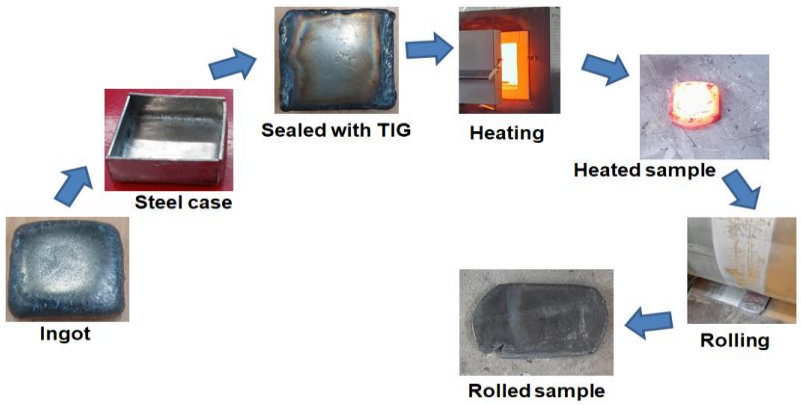

Figure 1: Schematic diagram of the hot-pack-rolling process.

2.3. Hardness measurements

Micro Vickers hardness tests were performed on the as-cast, as-rolled, and rolled and heat-treated specimens to obtain their hardness values. The specimens were prepared according to ASTM standard E3-11 for standard metallographic preparation. This involved grinding and polishing the samples using a 1 μm diamond suspension, followed by polishing with 50 nm colloidal silica. During the microhardness tests, a load of 500 gf was applied, and a dwelling time of 10 s was used, as required by ASTM standard E384–05a. The hardness values were given as the averages of at least 10 measurements taken at 0.5 mm intervals.

2.4. Plasticity testing

To determine the room-temperature tensile properties of the heat-treated sheet, a new technique called profilometry-based indentation plastometry (PIP) was employed. This technique uses a Plastometrex indentation plastometer to obtain plastic stress-strain curves. Specimen preparation for the test was carried out by mounting and polishing to a 1 μm finish. The sample was then set on the plinth of the plastometer. The WC-Co cemented carbide spherical indenter of radius 1 mm was used to produce the indent, using a force of 4.5 kN. A total of three tests was performed on the specimen.

2.5. Materials characterisation

The elemental powders, the as-cast ingot, and the rolled sheet were analysed on a Zeiss Axio Imager.M2 light microscope (LM) and a JEOL® JSM-6510 scanning electron microscope (SEM) in backscattered electron (BSE) mode. The obtained LM and SEM-BSE images of the cast and rolled samples were used to determine the average grain sizes by using the line intercept method in ImageJ software. To analyse the structural phase evolution in the rolled specimens, the X-ray diffraction technique was employed using the parameters Cu Kα radiation λ = 1.54062 Å and 2θ from 20° to 90° [4], [8]. Both the LM and the SEM-

BSE specimens for microstructural analysis of the as-cast ingot and rolled sheet were metallographically prepared by using the procedure explained in [8].

The powders were characterised to blend different particle sizes and morphologies. The particle size distributions of both the elemental powders and their mixture were measured using a Microtrac Bluewave laser diffraction particle analyser. To quantify the porosity in the compact and the ingot, the densities of the as-compacted and as-melted alloy parts were measured using the Archimedes method according to ASTM B962-08. The density values were then compared with a reference value reported in [10].

3. RESULTS AND DISCUSSION

3.1. The blending of powder characteristics

The SEM images shown in Figure 2a-f reveal the different morphologies of the elemental powders that were used in the fabrication of the sheet. It is evident that Ti and Nb powder particles indicate an irregular shape with ImageJ measured mean particle sizes of 31.25 and 74.83 μm respectively. Al particles show a spherical shape, and their average particle size is 36.17 μm, while Si and Cr particles show an angled-irregular shape with mean particle sizes of 8.12 and 101.24 μm respectively. In Figure 2f it appears that, during the blending and mixing, the ultra-fine particles of Si were attracted to the coarse particles of Al. This could be ascribed to the fact that the electrostatic forces between particles increase with decreasing particle size. The powder particle morphologies and their mean particle sizes are summarised in Table 1.

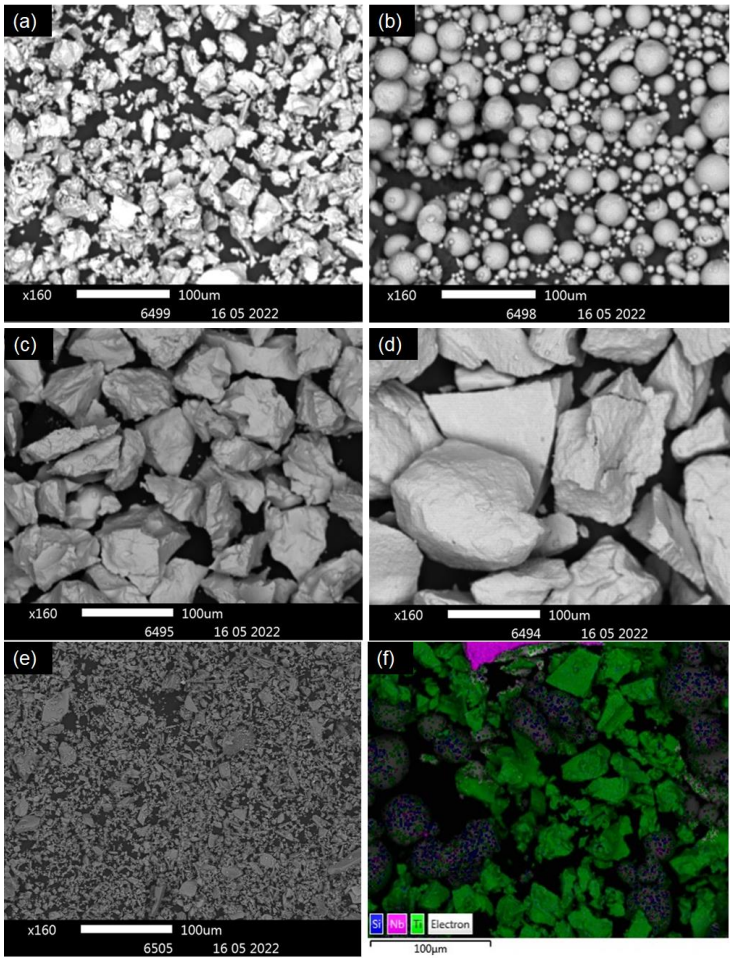

Figure 2: SEM micrographs of (a) Ti, (b) Al, (c) Nb, (d) Cr, (e) Si and (f) EDS layered image of blended and mixed powder particles

As pointed out by Jakub et al., [11] having different particle shapes in a powder charge affects the flowability properties of the powders during mixing and compacting in a die. Spherical-shaped metal particles exhibit better flow properties and a lower porosity than irregular ones owing to a reduction in surface friction and a lower risk of mechanical interlocking. This easy flowing of spherical particles promotes efficient packing, leading to higher bulk densities [12]. However, the free-flowing powder blends and mixtures might readily segregate upon subsequent handling, especially if the different components of the mixture do not adhere to one another [4]. In addition, the cost of highly spherical metal powders is substantially higher than those containing particles that are more irregularly shaped. Moreover, irregular-shaped particles have more irregularities on their surfaces that could interlock mechanically during pressing and so improve the strength of the green compact. Increased powder sphericity improves powder packing and flowability, but has an opposite effect on compressibility and the resulting green strength. Therefore, a compromise must be sought among powder morphologies. The optimum balance for these properties can be obtained by mixing powder particles of different shapes.

Figure 3a-b shows the cumulative particle size distributions (in wt%) of the elemental powders as well as the mixture measured using a Microtrac Bluewave laser diffraction particle analyser. The results seem to correlate with the ImageJ analysis. The D10, D50, D90, and span values for the elemental powders are also summarised in Table 1.

Table 1: Characteristics and particle size distribution parameters of precursor powders

Precursor powder	Mean particle size (μm)	Morphology	D10 (μm)	D50 (μm)	D90 (μm)	Span
Ti	31.25	Irregular	15.40	31.26	52.22	1.18
Al	36.17	Spherical	22.69	37.15	58.47	0.96
Nb	74.83	Irregular	52.33	75.29	109.20	0.76
Cr	101.24	Angular	51.91	103.2	164.10	1.09
Si	8.12	Angular	2.62	8.65	31.64	3.36

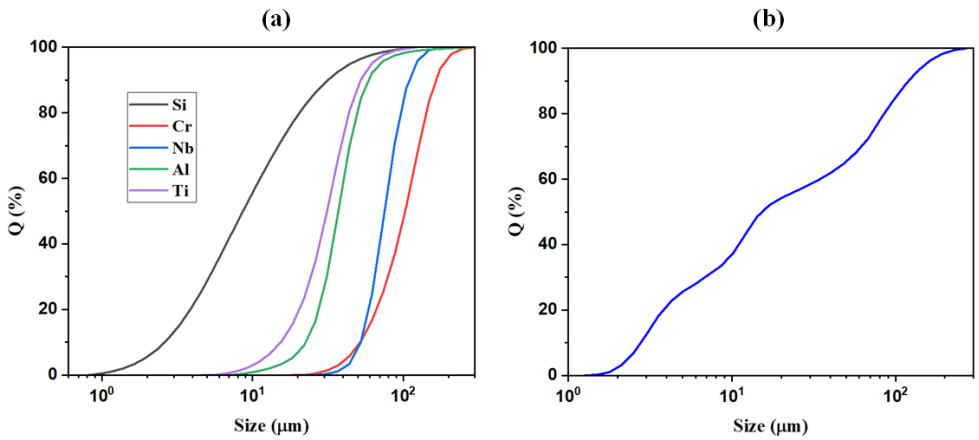

Figure 3: Cumulative particle size distributions in wt% (a) Precursor powders (b) TiAlNbCrSi mixed powders

As observed in Figure 3 and Table 1, Nb powder shows a narrow particle distribution compared with Ti, Al, Cr, and Si powder particles, which exhibit broader particle size distributions, with Si powder showing the widest of all. Furthermore, the mixture of the elemental powders appears to yield a trimodal distribution (Figure 3b), which is essential for the minimisation of shrinkage in the final ingot [13]. This increase in the polydispersity of the powder particles tends primarily to influence the compressibility of the powders in the die [11]. Thus, it helps the packing density to reach its maximum level during compaction by allowing the finer particles to fill the gaps left by the larger ones [14], thereby minimising the amount of pores in the green compact.

3.2. Density analysis of the compact and the button-ingot

The relative green density of Ti-48Al-2Nb-0.7Cr-0.3Si compact is compared with the ones of the γ-TiAl-based alloys that were studied in [4], as shown in Figure 4a. The compact and alloy density results are depicted on the primary and secondary axes respectively. The results indicate that the Ti-48Al-2Nb-0.7Cr-0.3Si compact possesses the highest relative green density. This significant improvement in the compact density could be regarded as a successful outcome of blending powders having different morphologies and a considerable size difference between them, which tends to aid in the mean packing densities during compaction [4]. However, the evaluation of the gradual progression of density from the precursor powders to the green compact was beyond the scope of this study.

The resulting cast button-ingot is illustrated in Figure 4b. It is evident that, as expected, the shrinkage cavities on the ingot are almost negligible. The relative density results of the ingot shown in Figure 4a indicate a value very close to 100%; and, comparing its results with those for the alloys studied in [4], the level of porosity in the alloy studied here was significantly reduced.

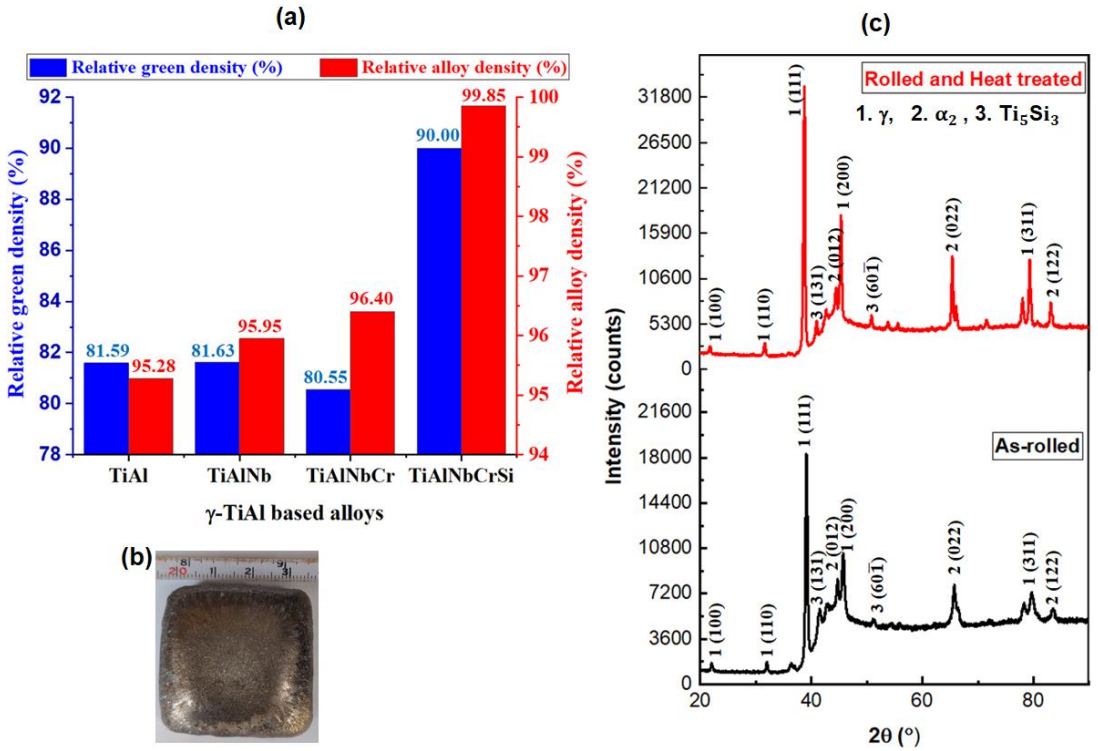

Figure 4: (a) Relative densities of the green compacts and the arc-melted buttons (TiAl, TiAlNb and TiAlNbCr density results were reproduced from [4] with permission from Elsevier); (b) macrograph of as-cast button-ingot; (c) XRD patterns of as-rolled and rolled and heat-treated Ti-48Al-2Nb-0.7Cr-0.3Si alloy

3.3. Analysis by x-ray diffraction (XRD)

Both the as-rolled and the rolled and heat-treated specimens were analysed by x-ray diffraction technique to study the structural phase evolution after the rolling and heat treatment, as shown in Figure 4c. It is clear that the patterns are identical for both specimens. All of the major phases for the alloy, such as γ (TiAl), α_2 (Ti_3Al), and titanium silicate (Ti_5Si_3), were reflected. Nevertheless, for as-rolled, some of the peaks were not distinctly reflected, and the pattern displays some sort of peak broadening. This implies that there was still some retained strain after hot rolling [15].

3.4. Microstructure characterisation of the as-cast and hot-rolled alloy

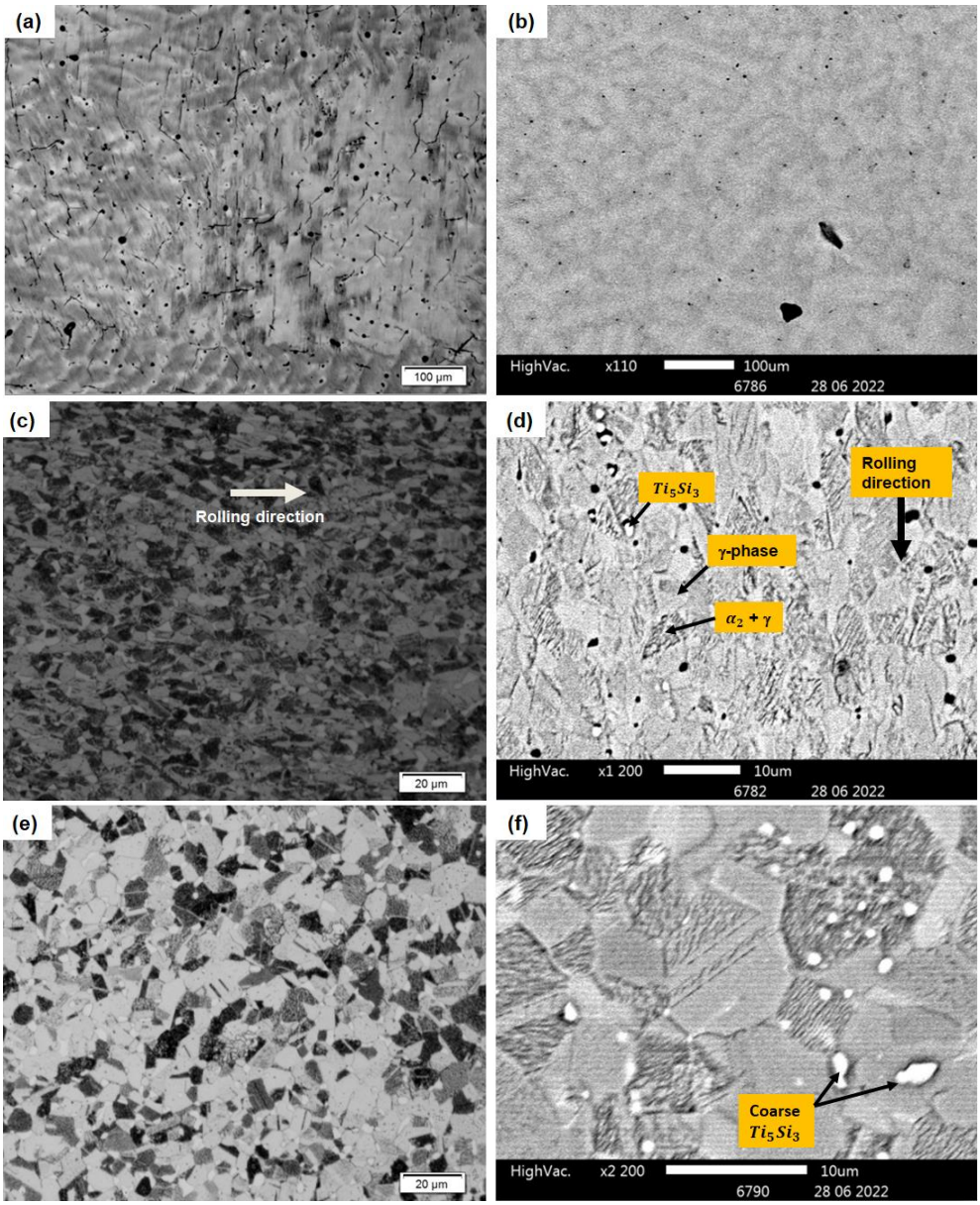

Figure 5: LM (LHS) and SEM-BSE (RHS) micrographs of Ti-48Al-2Nb-0.7Cr-0.3Si alloy (a) and (b) as-cast, (c) and (d) as-rolled sheet, (e) and (f) rolled and heat treated at 1250 °C for one hour

In the as-cast condition, the microstructure of Ti-48Al-2Nb-0.7Cr-0.3Si consists of inhomogeneous dendritic structures that are made of many small parts that look like cells, as shown in Figure 5a-b, and also as reported in [16]. This is ascribed to the tendency of Nb and Cr micro-segregating to the core of a solidifying dendrite during the solidification process. As Ti, Nb and Cr segregate to the emerging dendrites, the Al diffuses to the inter-dendritic regions. As may be observed in Figure 5a-b, both fine and coarse grains are present in the microstructure, although not well-defined, with an estimated mean grain size of 133 μm.

During hot-rolling, plastic stresses activate the movement of dislocations in the material; and, as observed by Xu et al., [17] the dislocations interact with defects such as vacancies and interstitials. With more stress being applied, the dislocations pile up along the initial grain boundaries until the boundaries become wavy and break down to form new grains by the process of dynamic recrystallisation or meta-dynamic recrystallisation [5], [18]. As can be seen in Figure 5c-d, the initial cellular-like dendritic structures observed in the as-cast microstructure (Figure 5a-b) collapsed to form the typical 'duplex' microstructure consisting of γ-phase, lamellar colonies of γ and α_2-phases as well as a small amount of titanium silicate (Ti_5Si_3) precipitates, as the diffusion process was restricted owing to the high rate of cooling in air. It is noteworthy that the resulting grains are very fine with an average grain size of 5 μm, and that they are slightly elongated along the rolling direction, as shown in Figure 5c-d.

Figure 5e-f shows that, when the rolled sheet was heat-treated at 1250 °C for one hour and cooled slowly in the furnace, grain growth occurred, as evidenced by the increase in their mean grain size to about 9 μm. Furthermore, the lamellar colonies became more equiaxed, and the number of titanium silicates increased. Moreover, some of the Ti_5Si_3 precipitates began to coarsen, as illustrated in Figure 5f. This can be attributed to the fact that, during heat treatment, coarsening mechanisms were activated.

3.5. Mechanical properties

The mechanical properties such as hardness, strength, and ductility in a metallic material are related to the grain size of its microstructure. Generally, fine grains result in high hardness and strength [8]. The relationship between the Vickers micro-hardness (plotted on the primary axis) and the corresponding ImageJ measured grain sizes (secondary axis) of the as-cast, as-rolled, and rolled and heat-treated alloy is shown in Figure 6a. The as-rolled specimen possesses the highest hardness of about 490 HV owing to its fine dynamically recrystallised grains. This hardness value dropped to about 398 HV after heat-treating the rolled sample. The drop in the hardness might be owing to the increase in grain size as a result of the heat treatment. Nevertheless, as shown in Figure 4c, the as-rolled sample displayed peak broadening, which implies that strain hardening might also be a contributing factor to the high hardness value shown in Figure 6a. In the as-cast condition, the alloy exhibited the lowest hardness value of about 362 HV. However, comparing this value with 323 HV obtained in [8] for a similar alloy called quinary, the hardness of the alloy in this study was improved.

Figure 6b shows the plastic stress-strain curve for the rolled and heat-treated specimen obtained from the indentation plastometry. The recorded yield stress was about 600 MPa, which correlates with the results reported in [5] for a high Nb-TiAl sheet; and, as illustrated in Figure 6b, a true plastic strain of about 3% and ultimate tensile stress of about 850 MPa can be obtained.

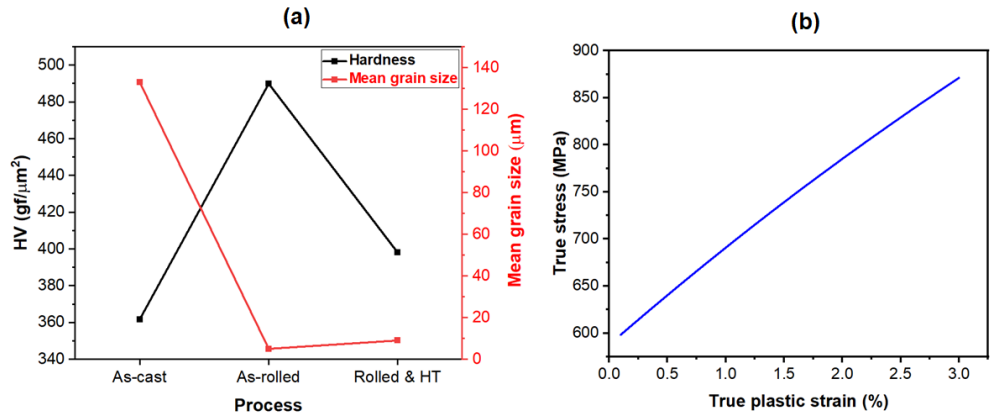

Figure 6: Mechanical properties of Ti-48Al-2Nb-0.7Cr-0.3Si (a) Micro-hardness and grain size of as-rolled, as-cast, and rolled and heat treated specimens; (b) Plastic stress-strain curve of rolled and heat treated specimen

4. CONCLUSION

The blending of precursor powders having different morphologies and a considerable size difference between them to produce a shrinkage cavity-free γ-TiAl-based ingot suitable for direct hot-pack rolling was investigated. From the investigation, the following conclusions are reached:

- Precursor powders of irregular, spherical, and angular shapes with an average particle size range of 8.12-101.24 μm were employed to fabricate the γ-TiAl-based alloy with nominal composition Ti-48Al-2Nb-0.7Cr-0.3Si through uniaxial cold-pressing of the powders, followed by arc-melting under vacuum atmosphere. The microstructure of the resulting ingot was found to contain a minimum level of porosity.
- It is possible to fabricate Ti-48Al-2Nb-0.7Cr-0.3Si alloy sheets directly from an as-cast ingot without performing intermediate heat treatment and thermo-mechanical processes, using the hot-pack rolling technique.
- Fine 'duplex' microstructure consisting of γ, $\gamma + \alpha_2$ lamellar colonies and precipitates of Ti_5Si_3 was produced by dynamic recrystallisation during hot-pack rolling. The microstructure was made uniform and more equiaxed by heat-treating the sheet at 1250 °C after hot-rolling, although the process resulted in slight grain growth. Improved mechanical properties were obtained from the resulting process.

5. ACKNOWLEDGEMENTS

The authors would like to acknowledge the Council of Scientific and Industrial Research for funding this work, and the University of Pretoria and Mintek for providing the laboratory equipment.

REFERENCES

[1] **D. M. Dimiduk**, "Gamma titanium aluminide alloys – An assessment within the competition of aerospace structural materials," *Mater. Sci. Eng. A*, vol. 263, no. 2, pp. 281–288, 1999.

[2] **S. R. Dey, A. Hazotte, & E. Bouzy**, "Crystallography and phase transformation mechanisms in TiAl-based alloys: A synthesis," *Intermetallics*, vol. 17, no. 12, pp. 1052–1064, 2009.

[3] **L. Yang, *et al.***, "Numerical simulation and experimental verification of gravity and centrifugal investment casting low-pressure turbine blades for high Nb-TiAl alloy," *Intermetallics*, vol. 66, pp. 149–155, 2015.

[4] **M. N. Mathabathe, A. S. Bolokang, G. Govender, C. W. Siyasiya, & R. J. Mostert**, "Cold-pressing and vacuum arc melting of γ-TiAl based alloys," *Adv. Powder Technol.*, vol. 30, no. 12, pp. 2925–2939, 2019.

[5] **Z. K. Shen, Z. Z. Lin, J. P. Liang, Y. F. Zhang, L. Q. Shang, & S. L. Liu**, "A novel hot pack rolling of high NbeTiAl sheet from cast ingot," *Intermetallics*, vol. 65, pp. 19–25, 2015.

[6] **G. Das, H. Kestler, H. Clemens, & P. A. Bartolotta**, "Sheet gamma TiAl : Status and opportunities," *JOM*, vol. 56, pp. 42–45, 2004.

[7] **H. Z. Niu, F. T. Kong, S. L. Xiao, Y. Y. Chen, & F. Yang**, "Effect of pack rolling on microstructures and tensile properties of as-forged Ti-44Al-6V-3Nb-0. 3Y alloy," *Intermetallics*, vol. 21, no. 1, pp. 97–104, 2012.

[8] **M. N. Mathabathe, A. S. Bolokang, G. Govender, R. J. Mostert, & C. W. Siyasiya**, "The vacuum melted γ-TiAl (Nb, Cr, Si)-doped alloys and their cyclic oxidation properties," *Vacuum*, vol. 154, pp. 82–89, 2018.

[9] **E. Schwaighofer, H. Clemens, J. Lindemann, A. Stark, & S. Mayer**, "Hot-working behaviour of an advanced intermetallic multi-phase γ-TiAl based alloy," *Mater. Sci. Eng. A*, vol. 614, pp. 297–310, 2014.

[10] **Y. W. Kim**, "Ordered intermetallic alloys, part III: Gamma titanium aluminides," *JOM*, vol. 46, no. 7, pp. 30–39, 1994.

[11] **J. Hlosta, D. Žurovec, L. Jezerská, J. Zegzulka, & J. Nečas**, "Effect of particle shape and size on the compressibility and bulk properties of powders in powder metallurgy," In *Met. 2016 – 25th Anniv. Int. Conf. Metall. Mater. Conf. Proc.*, 2016, pp. 1394–1399.

[12] **Malvern Panalytical** "Optimizing powder packing behaviour by controlling particle size and shape,"*https://www.malvernpanalytical.com/en/learn/knowledgecenter/Whitepapers/WP160610 OptimisingParticlePacking*, 23rd July 2022.

[13] **R. M. German**, *Particle packing characteristics*, 1st ed. Princeton NJ: Metal Powder Industries Federation, 1989.

[14] **J. Dawes, C. Langley, & J. Clayton**, "Optimizing metal powders for additive manufacturing: Exploring the impact of particle morphology and powder flowability," *Met. Powder Rep.*, vol. 69, no. 5, pp. 1–5, 2017.

[15] **J. G. M. van Berkum, A. C. Vermeulen, R. Delhez, T. H. de Keijser, & E. J. Mittemeijer**, "Applicabilities of the Warren-Averbach analysis and alternative analysis for separation of size and strain broadening," *J. Appl. Cryst.*, vol. 27, pp. 345–357, 1994.

[16] **M. N. Mathabathe, S. Govender, A. S. Bolokang, & R. J. Mostert**, "Phase transformation and microstructural control of the α-solidifying γ -Ti-48Al-2Nb-0.7Cr-0.3Si intermetallic alloy," *J. Alloys Compd*, Vol. 757, pp. 8–15, 2018.

[17] **D. S. Xu, H. Wang, & R. Yang**, "Point defect formation by dislocation reactions in TiAl," *IOP Conf Series: Mater. Sci. Eng.*, vol. 3, pp. 1–6, 2009.

[18] **W. Zhang, Y. Liu, H. Z. Li, Z. Li, H. Wang, & B. Liu**, "Constitutive modelling and processing map for elevated temperature flow behaviours of a powder metallurgy titanium aluminide alloy," *J. Mater. Process. Technol.*, vol. 209, pp. 5363–5370, 2009.